

## Corrosion behavior of Fe and Ni commercial alloys in direct-fired supercritical CO<sub>2</sub> power cycle environments

### Joseph H. Tylczak

Materials Research Engineer  
National Energy Technology Laboratory  
Albany, OR USA

[joseph.tylczak@netl.doe.gov](mailto:joseph.tylczak@netl.doe.gov)

### Richard P. Oleksak

National Energy Technology Laboratory  
and AECOM

Albany, OR USA

[richard.oleksak@netl.doe.gov](mailto:richard.oleksak@netl.doe.gov)

### Gordon R. Holcomb

Materials Research Engineer  
National Energy Technology Laboratory  
Albany, OR USA

[gordon.holcomb@netl.doe.gov](mailto:gordon.holcomb@netl.doe.gov)

### Ömer N. Doğan

Materials Research Engineer  
National Energy Technology Laboratory  
Albany, OR USA

[omer.dogan@netl.doe.gov](mailto:omer.dogan@netl.doe.gov)



*Joseph Tylczak is a Research Metallurgist Engineer in the Structural Materials Team in the Research & Innovation Center at NETL. He received his degree in Physical Metallurgy from Washington State University in 1979. His current work includes high temperature corrosion issues with advanced fossil fueled power systems and ambient temperature corrosion of gas transmission pipelines.*



*Richard Oleksak is an AECOM Research Scientist working with the Structural Materials Team at NETL. He received his Ph.D. from Oregon State University in Chemical Engineering in 2015. His current research focuses on understanding the oxidation and corrosion behavior of structural alloys for next-generation power systems.*



*Gordon Holcomb is a Materials Research Engineer in the Structural Materials Team in the Research & Innovation Center at NETL. He received his Ph.D. from the Ohio State University in Metallurgical Engineering in 1988. Current projects cover corrosion issues in fossil energy systems. He is the U.S. Lead for the Corrosion in Supercritical Fluids task in the US-UK Collaboration on Fossil Energy Research and Development, Advanced Materials Technology Area.*



*Ömer Doğan is a Materials Research Engineer in the Structural Materials Team in the Research & Innovation Center at NETL. He received his Ph.D. from Case Western Reserve University in Materials Science & Engineering in 1990. Current research focuses on the evaluation and development of heat, corrosion, and wear resistant materials for applications in harsh environments.*

## ABSTRACT

Materials degradation issues remain a primary concern for implementation of direct-fired supercritical CO<sub>2</sub> (sCO<sub>2</sub>) power cycles. Structural alloys must be identified which sufficiently resist oxidation/corrosion in high-temperature sCO<sub>2</sub>-rich environments. Recent studies have evaluated alloy performance in high-purity CO<sub>2</sub>, relevant for indirect power cycle configurations. Significantly fewer studies have considered the role of combustion impurities which will contaminate the working fluid and potentially dominate the corrosion behavior of structural alloys in direct cycle configurations. In this study, we exposed a variety of commercial Fe (Grade 22, Grade 91, 304H, 310S, 347H, E-Brite) and Ni (Inconel 617, Haynes 230, Inconel 625, Inconel 740H, Haynes 282, NIMONIC 263) alloys to high temperature CO<sub>2</sub> containing O<sub>2</sub> (1 vol %) and H<sub>2</sub>O (4 or 11 vol %) with and without SO<sub>2</sub> (0.1 vol %) to simulate the conditions expected for natural gas- and coal-fired direct sCO<sub>2</sub> power cycles. The alloys were exposed at 1 bar and 750 °C (Ni alloys) or 550 °C (Fe alloys) for up to 2,500 h. Presented are results of mass change, X-ray diffraction, and scanning electron microscopy analysis to establish the extent of corrosion in these environments. Gravimetric results indicate, after an initial high corrosion period, that most alloys showed a low ongoing corrosion rate. The individual Ni based alloys showed similar corrosion rates both with and without 0.1 vol % SO<sub>2</sub>. Results are used to assess the suitability of various commercial alloys for direct sCO<sub>2</sub> power cycle applications.

## INTRODUCTION

The desire to improve the efficiency of power generation has led to renewed interest in the use of a supercritical CO<sub>2</sub> Brayton power cycle in place of the conventional steam Rankine cycle. This sCO<sub>2</sub> cycle offers advantages, among them are increased thermal efficiency, smaller size, and lower materials costs. Thermodynamic advantages of this cycle have been described in the literature [1-3]. Most work on this cycle has explored the use of indirectly heating the CO<sub>2</sub> working fluid. A variety of power sources have been proposed for the indirect heating including nuclear, geothermal, fossil fuel combustion, and concentrated solar sources. While most of these heat sources would use indirectly heated CO<sub>2</sub>, the combustion of fossil fuels presents the opportunity for a direct fired CO<sub>2</sub> cycle where the combustion product is directly used to turn a turbine. One example of this is the Allam[4] cycle. While the indirect cycles use highly purified CO<sub>2</sub> for the recycled working fluid, the direct firing introduces additional combustion impurities into the stream. The direct cycle continues to have a large quantity of recycled CO<sub>2</sub>, with generated CO<sub>2</sub> matching the quantity of CO<sub>2</sub> removed from the cycle. Initial Allam cycle power plants are expected to use natural gas as a fuel, although there are conceptual designs using syngas from coal gasification as a fuel source.

Materials are often the limiting factor during power plant design. Designers face the decision of choosing the most economical alloy, which depends on where in the plant it is located, expected conditions, and the expected lifetime of the component. Both strength of the material and its corrosion resistance are paramount.

Materials of construction is an issue for both the indirect and direct fired sCO<sub>2</sub> power plants. Existing alloys have been generally designed for steam exposure. There is need to see if they are suitable for high temperature CO<sub>2</sub> exposure. While the oxygen potential is similar for high temperature CO<sub>2</sub> and H<sub>2</sub>O environments, the possibility of carburization presents additional concerns in high-temperature CO<sub>2</sub>. The combustion gas stream will also have some amount of excess oxygen, which is also expected to play a role in corrosion. Another expected contaminant is SO<sub>2</sub>. Natural gas may contain H<sub>2</sub>S, which would oxidize to SO<sub>2</sub> or SO<sub>3</sub> during combustion. Coal syngas will also have some sulfur in the gas stream, which will combust to SO<sub>2</sub>. These combustion gases should influence the corrosion rate of any metals downstream of the combustion.

Research by many groups has shown that the high temperature corrosion performance of conventional alloys in pure CO<sub>2</sub> is different than in air or steam [5, 6].

To help determine whether current alloys are appropriate for direct fired Allam cycle power plants this corrosion research on a variety of commercial iron and nickel based alloys was conducted.

## PROCEDURE

A variety of commercial high temperature Fe based and Ni based alloys, most with existing ASME boiler code acceptance, were chosen for this work. The Fe based include ferritic Grade (GR) 22 (UNS K21590), GR 91 (UNS K90901), E-Brite (UNS S44627) steels, and austenitic 304H (UNS S30409), 310S (UNS S31008), and 347H (UNS S34709) steels. The Ni based alloys include solution hardened alloys INCONEL 600 (UNS N06600), INCONEL 617 (UNS N06617), INCONEL 625 (UNS N06625), Haynes 230 (UNS N06230), and INCOLOY 800 (UNS N08800), age hardenable NIMONIC 263 (UNS N072263), Haynes 282 (UNS N07208), INCONEL 718 (UNS N07718), and INCONEL 740H (UNS N07740). The primary composition components of the alloys can be found in Table 1. The values are from either manufactures' analyses (P22, P91, 310S, 347H, 617, 625, 263, and 718) or in-house XRF analyses. These alloys depend primarily on Cr for their oxidation resistance. The Cr concentration ranges from a low of 2 ¼ wt. % Cr for the GR 22 ferritic steel to 26 wt. % for the E-Brite steel. Oxidation resistance is also enhanced by the additions of Al, Si, and Ti. The other additions are primarily added for improved mechanical properties.

Table 1. Composition of alloys evaluated in this work.

Alloy	Fe	Ni	Cr	Co	Mo	Mn	W	Nb	Si	Ti	Al	C
<b>Iron Based</b>												
<b>Ferritic</b>												
GR 22	95.5	0.15	2.29	--	0.94	0.52	--	0	0.21	0	0.03	0.13
GR 91	89.3	0.09	8.37	--	0.9	0.45	--	0.07	0.33	0	0.01	0.09
E-Brite*	71.6	0.21	26.5	0.02	1.0	0.04	<0.010	0.12	0.25	<0.001	0.1	--
<b>Austenitic</b>												
304H*	70.6	8.27	18.7	0.22	0.12	1.08	0.01	0.01	0.44	0	0.01	
310S	53.5	19.1	25	0.17	0.09	1.39	--	0.01	0.39	0	0.02	0.04
347H	70.1	9.01	17.3	0.14	0.37	1.86	--	0.52	0.31	0	--	0.05
<b>Nickel Based</b>												
<b>Solution strengthened</b>												
230*	0.4	59.8	22.2	0.34	1.26	0.51	14.39	0.04	0.44	0.01	0.42	--
600*	7.58	75	16	0.07	0.23	0.22	<0.010	0.11	0.15	0.33	0.14	--
617	0.39	55.1	21.9	11.45	9.61	0.04	<0.010	0.03	0.02	0.47	0.91	--
625	4.44	60.4	22.3	0.03	8.33	0.36	--	3.5	0.23	0.19	0.14	0.08
800*	44.2	32.7	19.9	0.07	0.2	0.91	<0.010	0.05	0.46	0.46	0.37	--
<b>Age Hardenable</b>												
263	0.42	50.7	20.3	19.65	5.84	0.35	--	0.08	0.02	2.18	0.39	0.06
282*	0.15	58.2	19.3	12.12	8.44	0.08	--	0.02	0.17	2.13	1.29	--
718	18.1	53.8	18	0.16	3.03	0.24	--	5.3	0.08	1.02	1.55	0.05
740H*	<0.010	50.4	24.5	20.2	0.31	0.24	<0.010	1.53	0.12	1.38	1.2	--

Compositions in wt. %. Values for alloys marked with a \* were from in-house XRF

Coupons of the various alloys were prepared by machining larger commercial materials into test coupons, with general dimensions of 19 x 12.5 x 2 mm. A typical coupon is shown in Figure 1. The coupons were made from plate or sheet stock. The coupons had a hole drilled in the upper center, about 5 mm from the top, used for hanging from during testing. The coupons surfaces were finished by lapping, using 17.5 µm alumina, and then hand finishing using a 600-grit silicon carbide paper. After mechanical preparation, the coupon dimensions were measured and recorded,

then they were cleaned, dried, and weighted to a precision of  $\pm 0.01$  mg. Pairs of coupons were hung in non-adjacent locations on a metallic rack constructed from alloy 617 during their exposure in the tube furnaces. With the sparse amount of rack construction material and the constant gas flow past the coupons it was judged the rack and adjacent test materials would have minimal effect on the results. No change in character of the corrosion was noted in or near the hole where the coupon was hung. The tube furnaces were electrically heated 3-zone tube furnaces with mullite tubes and sealing endcaps. Figure 2 shows a coupon rack sitting on one of the tube furnace between exposure runs. The image shows the relative packing design and density of the coupons, relative to each other and to the rack. Prior to exposure the furnaces were temperature profiled for the conditions used for the exposures, 750 °C for the Ni alloys and 550 °C for the Fe based alloys, to ensure exposure temperature uniformity.



Figure 1. Image of a typical coupon prior to exposure. In picture scale is in inches.

The racks of coupons were loaded into center of the tube furnaces and endcaps applied to the tubes to seal them. Carbon dioxide was flowed through the tubes prior to high temperature exposure to purge them of residual air. Gas conditions were created by mixing research grade (99.999 %) CO<sub>2</sub> with grade B (99.5 %) O<sub>2</sub>, and for some exposures anhydrous (99.98 %) SO<sub>2</sub>, prior to the gases introduction to the tube. For the tests with SO<sub>2</sub> additions, the gas was introduced into a hot section of the furnace after flowing over a Pt/Rh mesh intended to catalyze the conversion of SO<sub>2</sub> to SO<sub>3</sub>. High purity "Type 1" water was introduced as liquid water and flashed to steam in the tube. The volume of gases, and steam, were such that there was a gas flow of 25 cm/min (at temperature) past the coupons. Three different gas conditions with two temperatures were used for these tests and detailed in Table 2. These conditions are abbreviated as DF11, DF4-L, DF4S-L, DF4-H and DF4S-H; identifying the amount of water in the gas stream, whether SO<sub>2</sub> was added and whether this was a low (550 °C) or high (750 °C) temperature condition. All the DF11 testing was done at 750 °C. These DF11 tests included Ni based alloys. For the lower 4 vol % water tests, the Ni based alloys were tested at 750 °C and the Fe base alloys at 550 °C.



Figure 2. Rack of test coupons resting on top of one of the tube furnaces prior to reloading for additional exposure testing.

Table 2. Test conditions of exposure tests.

Condition	CO <sub>2</sub> , vol %	O <sub>2</sub> , vol %	SO <sub>2</sub> , vol %	H <sub>2</sub> O, vol %	Temp, °C
DF11	88	1	--	11	750
DF4-L	95	1	--	4	550
DF4S-L	95	1	0.1	4	550
DF4-H	95	1	--	4	750
DF4S-H	95	1	0.1	4	750

To start a test, a furnace was heated at 200 °C/h to the select temperature. When the furnace interiors reached the test temperature the remaining gases and water were started, and the exposure time recorded. Generally, after every 500 h the test was interrupted. The gases other than CO<sub>2</sub> were stopped and the tube furnace was cooled, initially at 200 °C/h, in flowing CO<sub>2</sub>. After reaching room temperature the coupon rack was removed from the furnace and the coupons reweighed, again to a precision of ±0.01 mg. After reaching a total of 2,500 h of exposure one coupon of each type was removed for analysis. This analysis included glancing angle x-ray diffraction (XRD), surface scanning electron microscopy (SEM), and for the Ni alloys DF4-H and DF4S-H tests, cross sectioning followed by SEM examination.

## RESULTS

### Visual Examination

Following each step of the exposure testing the coupons showed a visible increasing buildup of scale. The coupons exposed in the atmosphere with 0.1 vol % SO<sub>2</sub> were visibly more scaled than those without SO<sub>2</sub>. At the end of 2,500 h of exposure in the DF4-L condition as seen in Figure 3, most of the Fe based alloys had a straw or green tint which retained a metallic shine indicating only a very thin surface layer of oxide or scale. The exceptions to this were the GR 22 and 91 alloys, which showed a rough gray to black surface with hints of some loosely attached surface scale. The Fe alloys in the DF4S-L atmosphere with the SO<sub>2</sub> were darker, as seen in Figure 4. These alloys all showed rough surfaces which ranged in color from a light gray, to reddish, to dark grey/black.

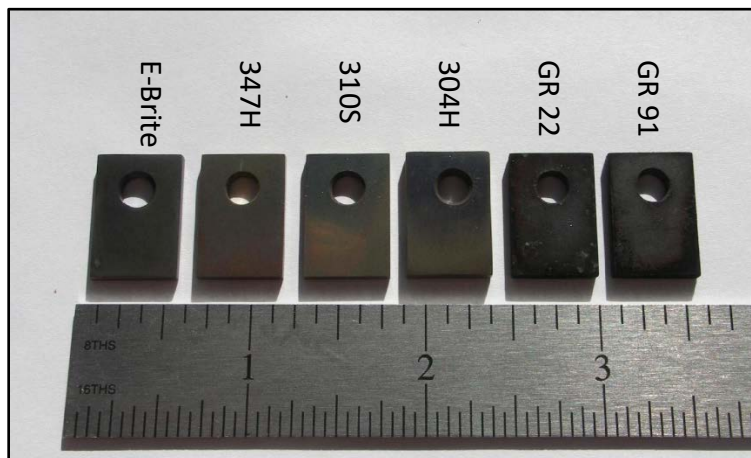


Figure 3. Image of DF4-L Fe based alloys after 2,500 h of exposure. In picture scale is in inches.

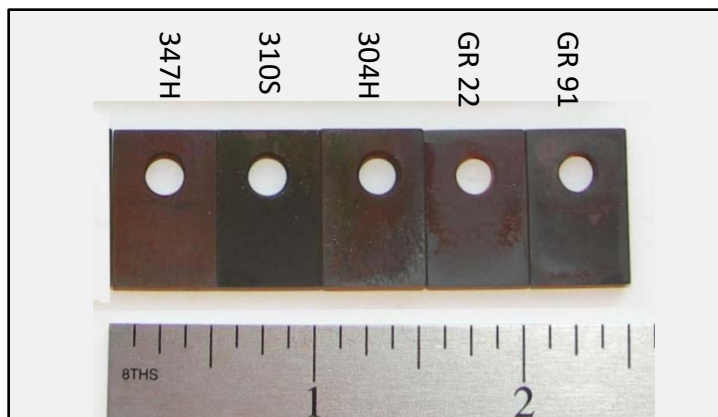


Figure 4. Image of the DF4S-L Fe based alloys after 2,000 h of exposure. In picture scale is in inches.

For the Ni alloys in both the DF11 and DF4-H condition at 2,500 h of exposure showed a mostly smooth adherent dark grey to black surface as seen in Figure 5. An exception was the 263, which showed signs of having a top darker loosely adherent surface scale over a lighter lower scale.

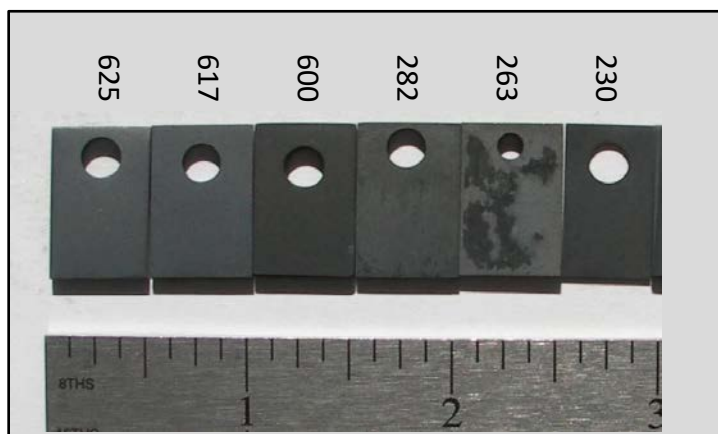


Figure 5. Image of DF4-H Ni based alloys after 2,500 h of exposure. In picture scale is in inches.

The Ni based alloys exposed in the DF4S-H atmosphere, as seen in Figure 6, with the SO<sub>2</sub> added, showed a rougher surface than DF4-H Ni alloys. The surfaces showed colors ranging from a light gray, for the 263, to darker grays to black, some with a hint of green. The Alloy 800 showed a reddish cast, possibly from Fe<sub>2</sub>O<sub>3</sub> corrosion product. Some alloys showed a fine silvery specking on their surfaces.

While we attempted to keep the exposure conditions uniform, pairs of coupons did not show identical surfaces after exposure. The coupons were hung so one coupon of an alloy might be at the front outside of the exposure rack while its mate might be in the center of the exposure rack, and furnace. While the surfaces of the coupons visually varied the gravimetric measurements between paired coupons were generally close.

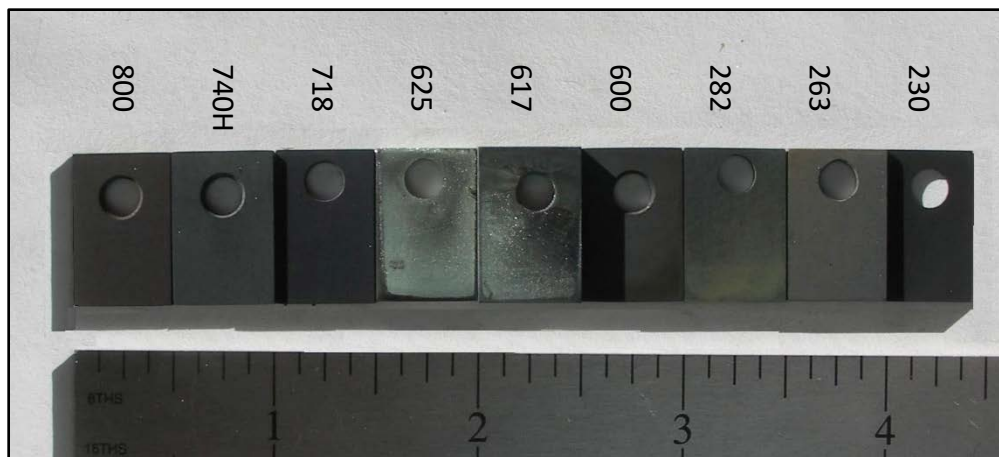


Figure 6. Image of DF4S-H Ni based alloys after 2,500 h of exposure. In picture scale is in inches.

### Gravimetric measurements

The coupons were removed from the furnace and weighed after every 500 h of exposure. The Fe, ferritic alloys were only exposed at DF4-L and DF4S-L (550 °C). The lower Cr GR 22 and 91 alloys, Figure 7, showed a significant mass gain in the first 500 h of exposure for both the DF4-L and DF4S-L conditions. The GR 91 steel showed about 10 % lower mass gain than the GR 22 steel. After the initial 500 h exposure, the ongoing mass gain was linear. As mentioned in the visual examination, the coupons in the environment with SO<sub>2</sub> appeared more heavily corroded than the coupons without SO<sub>2</sub>, while the gravimetric data showed very similar results for the alloys. At 2,500 h of exposure The GR 22 steel alloy in either environment had over 8 mg/cm<sup>2</sup> of mass gain and the GR 91 at just over 7 mg/cm<sup>2</sup>. The austenitic Fe based alloys (and E-Brite), with their higher Cr content, Figure 8, performed significantly better. The alloys in the DF4-L environment, no SO<sub>2</sub> addition, showed only minor mass change, with the worst, 347H gaining  $\approx 0.04$  mg/cm<sup>2</sup> after 2,500 h and the best, E-Brite gaining  $\approx 0.004$  mg/cm<sup>2</sup>. This corresponds to the visual examination that showed just thin interference colored oxide films. These alloys in the DF4S-L environment had a measurably higher corrosion rate at 500 h and, for the alloys with the lowest Cr content (304H and 347H) showed signs of breakaway corrosion after between 1,000 and 1,500 h of exposure. The 347H gained  $\approx 0.49$  mg/cm<sup>2</sup> over 2,250 h while the 304H gained  $\approx 0.62$ . The other two alloys with higher Cr (310S and E-Brite) had less than 0.2 mg/cm<sup>2</sup> mass gain after 2,500 h of exposure.

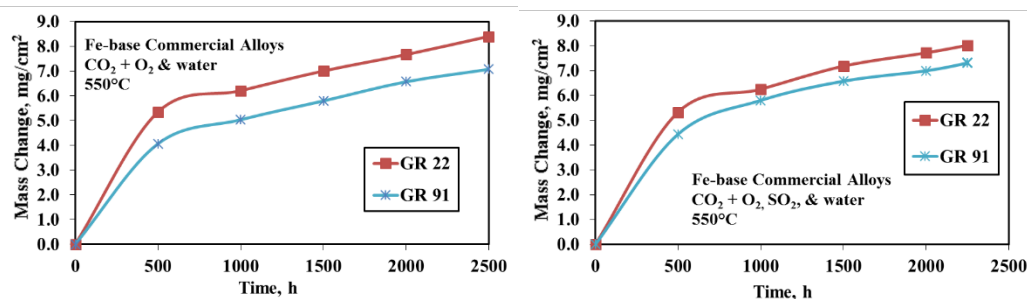


Figure 7. Gravimetric results for the oxidation of Fe based ferritic GR 22 and GR 91 alloys in direct fired gas conditions at 550 °C. The left-hand figure shows the results for coupons without added SO<sub>2</sub>, the figure on the right shows the results for coupons with SO<sub>2</sub> added to the gas stream.

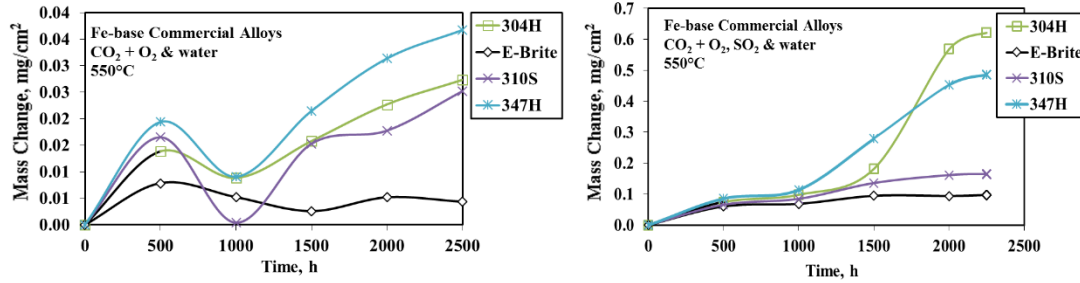


Figure 8. Gravimetric results for the oxidation of Fe based austenitic alloys in direct fired gas conditions at 550 °C. The left-hand figure shows the results for coupons without added SO<sub>2</sub>, the figure on the right shows the results for coupons with SO<sub>2</sub> added to the gas stream.

The Ni based alloys were exposed to three conditions, DF11, DF4-H, and DF4S-H, all of which were at 750 °C. There was not a uniformly most or least aggressive conditions, rather it depended on the alloy and the alloying additions it contained.

For the high water DF11, Figure 9, two alloys stood out for the highest mass gain, from the worst to next worst, were alloys 263 (1.12 mg/cm<sup>2</sup> after 2,500 h) and 800 (0.90 mg/cm<sup>2</sup> after 2,500 h). These, plus the 740H were still showing significant mass gains, exposure to exposure at 2,500 h. The alloy with the least mass gain was the alloy 625, with only a gain of 0.03 mg/cm<sup>2</sup> after 2,500 h. The alloy 625 and the remaining alloys, 617, 230, and 600, showed relatively constant mass after the first 1,000 h of exposure, with the difference being the initial mass gains.

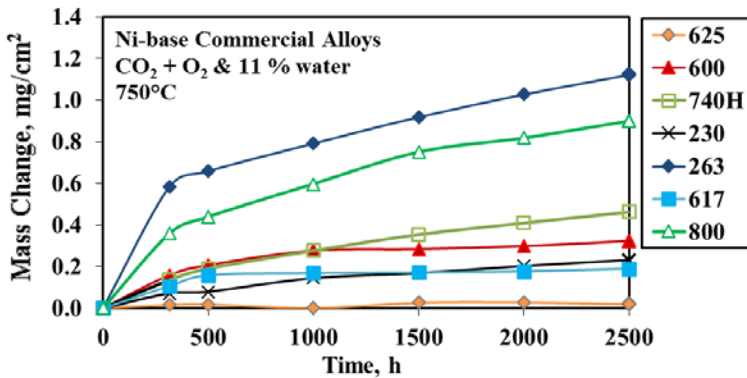


Figure 9. Gravimetric result for the oxidation of Ni based alloys in a high, 11 vol %, water direct fired gas condition at 750 °C.

For the lower water DF4-H, Figure 10, without SO<sub>2</sub> additions, the alloy 800 stood out for the highest mass gain, at 1.31 mg/cm<sup>2</sup> after 2,500 h. Next worst was 263 with a mass gain of 0.95 mg/cm<sup>2</sup> after 2,500 h. This alloy had been the worst with the highest water. It is possible if this alloy was not suffering spallation, seen in Figure 5, thus losing mass, that this alloy might have had the highest mass gain. The alloy 282 stands out as the alloy with the third highest mass gain. The alloy with the least mass gain was alloy 230, which gained 0.18 mg/cm<sup>2</sup> after 2,500 h. Other alloys that showed low mass gain included 625, 600, 740H, 718, and 617.

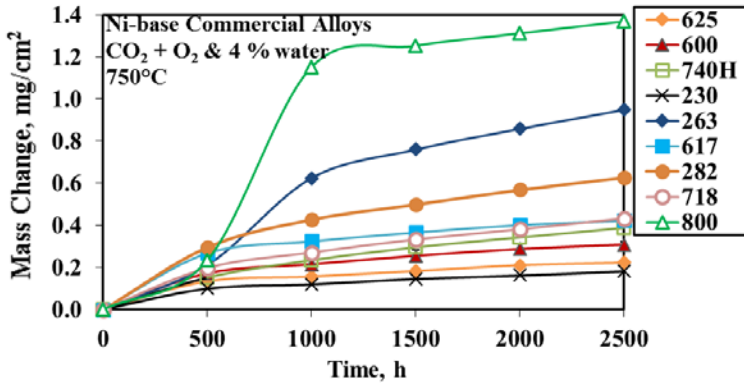


Figure 10. Gravimetric result for the oxidation of Ni based alloys in a moderate, 4 vol % water direct fired gas condition with no SO<sub>2</sub> at 750 °C.

For the low water DF4S-H, Figure 11, with SO<sub>2</sub> additions, (like the high water DF11 exposure) the alloy 263 had the highest mass gain, at 0.92 mg/cm<sup>2</sup> after 2,500 h. Like the highest water exposure, the alloy 800 had the next highest mass gain, at 0.69 mg/cm<sup>2</sup> after 2,500 h. Next there is a cluster of three alloys, 282, 617, and 740H with similar mass gains (from 0.55 mg/cm<sup>2</sup> after 2,500 h for the 282 to 0.45 mg/cm<sup>2</sup> after 2,500h for the 740H). Gaining the least mass were alloys 230, 625, 600, 718 (with 230 gaining 0.19 mg/cm<sup>2</sup> after 2,500h to 718 gaining 0.33 mg/cm<sup>2</sup> after 2,500 h.)

For all three of these conditions the age hardenable 263 and high Fe content 800 had high relative mass gains. As will be seen below this corresponds to a thick surface scale. The solid solution alloys 230, 625, and 600 had low relative mass gains and thin surface scales.

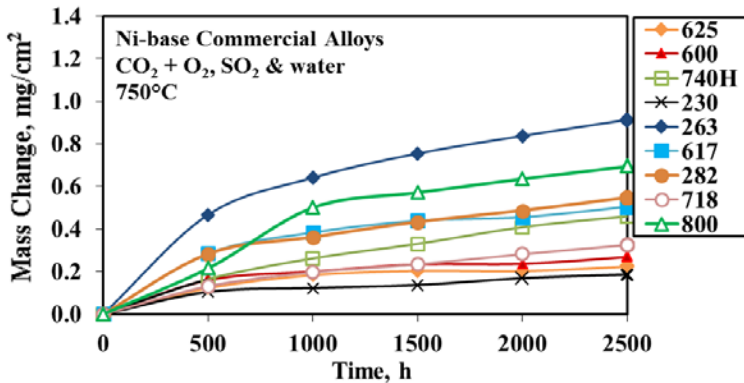


Figure 11. Gravimetric result for the oxidation of Ni based alloys in a moderate, 4 vol % water direct fired gas condition with SO<sub>2</sub> at 750 °C.

## X-ray Diffraction

The Ni based alloys were examined by glancing angle XRD[7] after 2,500 h of exposure. For this work a X-ray incidence angle of 2 ° was used. They all showed a significant layer of Cr<sub>2</sub>O<sub>3</sub> on the surface. Both Al<sub>2</sub>O<sub>3</sub> and TiO<sub>2</sub> were found in alloys containing the corresponding Al or Ti additions. Time constraints limited XRD to the Ni alloys for this proceeding. The Ni and Fe based alloys will be further examined in subsequent works.

## SEM Examination

Surface SEM was performed on some of the Fe alloys. As described in the visual examination of the Fe alloys, there was a substantial difference in appearance between the alloys exposed in the DF4-L and DF4S-L conditions. This

difference extended to the SEM observations. The GR 91 alloy in the DF4-L condition, Figure 12 left, showed a tight uniform top scale that was separating from the material below. This was producing large pieces of scale. This scale loss would have limited the gravimetric mass gain of this coupon. The coupon exposed in the DF4S-L condition showed a much rougher surface and signs of a continuously failing and regenerating surface. This resulted in a surface of scale nodules and fine plate like crystals. Energy dispersive X-ray spectroscopy (EDS) analysis of the surface showed a composition of Fe oxide, with 1.1 wt. % Si, and 0.7 wt. % S.

The austenitic steels exposed in the DF4-L condition at 550 °C, like the 310H shown in Figure 13 left, while exhibiting charging characteristics of having an electrically insulating oxide film, showed little more than the original metallic surface for the coupon with no scale seen at this magnification. The original grinding scratch marks are still visible in the image. In contrast, the coupon exposed in the DF4S-L condition, Figure 13 right, shows signs of its top scale surface failing and producing fine blocky oxide scale of  $\approx 10$  to 30  $\mu\text{m}$  diameter. EDS analysis of the surface showed its composition was mostly (Fe Si) oxide with 2.7 at. % S.

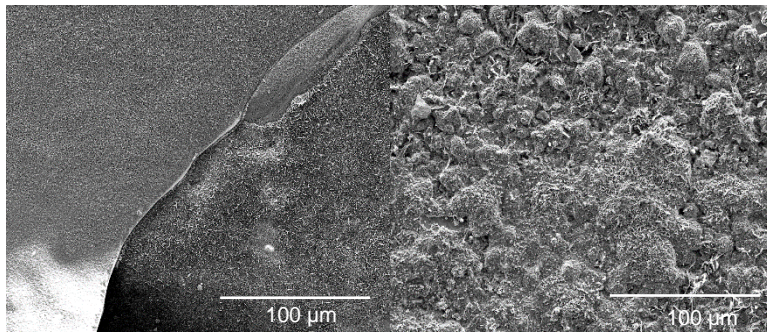


Figure 12. Surface SEMs of GR 91 steel, left hand image of coupon exposed in DF4-L condition at 550 °C, right hand coupon was exposed in DF4S-L condition at 550 °C. The coupons were imaged after 2,500 h. of exposure for the DF4-L condition and 2,250 h. for the DF4-H condition.

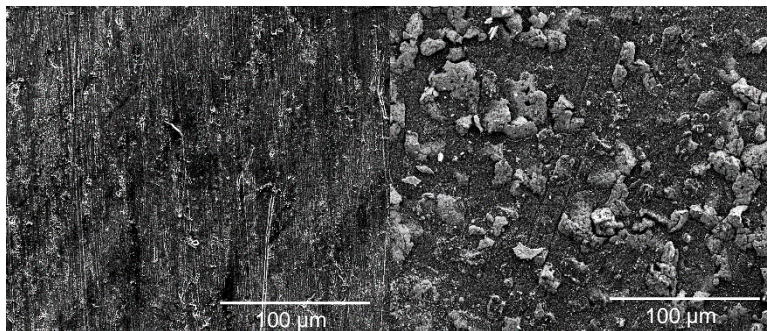


Figure 13. Surface SEMs of 310H steel, left hand image of coupon exposed in DF4-L condition at 550 °C, right hand coupon was exposed in DF4S-L condition at 550 °C. The coupons were imaged after 2,500 h. of exposure for the DF4-L condition and 2,250 h. for the DF4-H condition.

Further exposure testing and evaluations of both the Fe and Ni based alloys is an ongoing process. Cross sections of the Fe based alloys were not yet available when this manuscript was completed.

Both surface and cross-sectional SEM analysis was performed on many of the Ni alloys. Figure 14 shows SEM results of alloy 230, which displayed the lowest mass gain among the Ni alloys exposed to the DF4-H and DF4S-H environments.

EDS analysis of the surface and cross-sections confirmed that a continuous Cr-rich oxide layer had formed during exposure to both DF4-H and DF4S-H. Nodules of Mn-rich oxide were observed on the surface of the coupon exposed

to DF4-H (Figure 14a). These nodules were absent in the coupon exposed to DF4S-H, however slight Mn-enrichment was observed in thicker regions of the Cr-oxide layer (Figure 14c).

An additional feature is shown in the cross-sections which was observed for all Ni alloys exposed to these environments. Interfacial voids are seen at the oxide/alloy interface, and in some cases the voids appear to be partially filled with oxide. It has been proposed that these voids are created by the condensation of metal vacancies formed as Cr leaves the alloy during growth of the oxide layer. [8, 9]

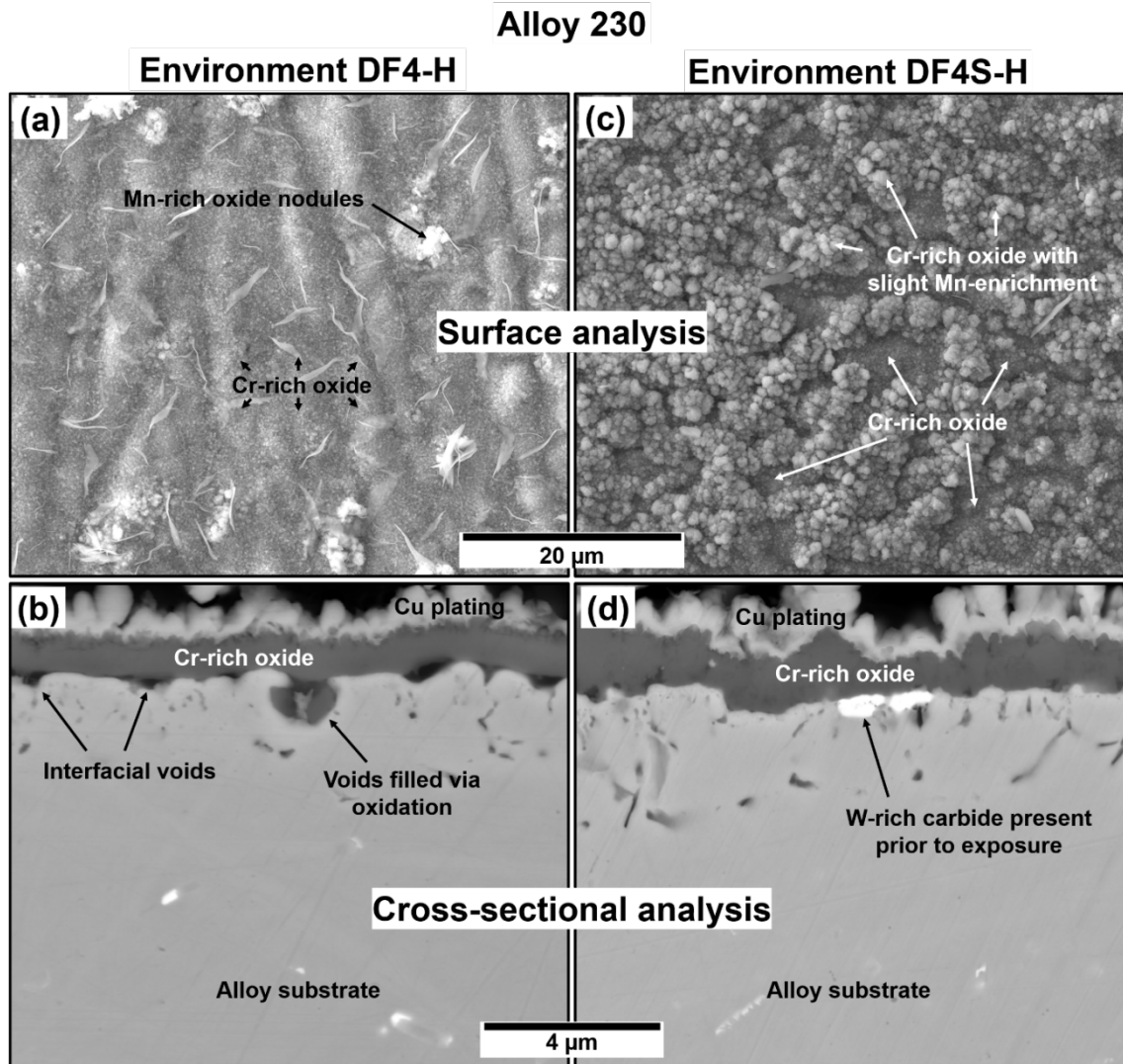


Figure 14. SEM analysis of alloy 230. (a-b) SE surface image and BSE cross-sectional image of coupon exposed to environment DF4-H. (c-d) SE surface image and BSE cross-sectional image of coupon exposed to environment DF4S-H. Both coupons imaged after 2,500 h. of exposure.

Figure 15 shows SEM results of 263, which displayed among the highest mass gains for Ni alloys exposed to environments DF4-H and DF4S-H.

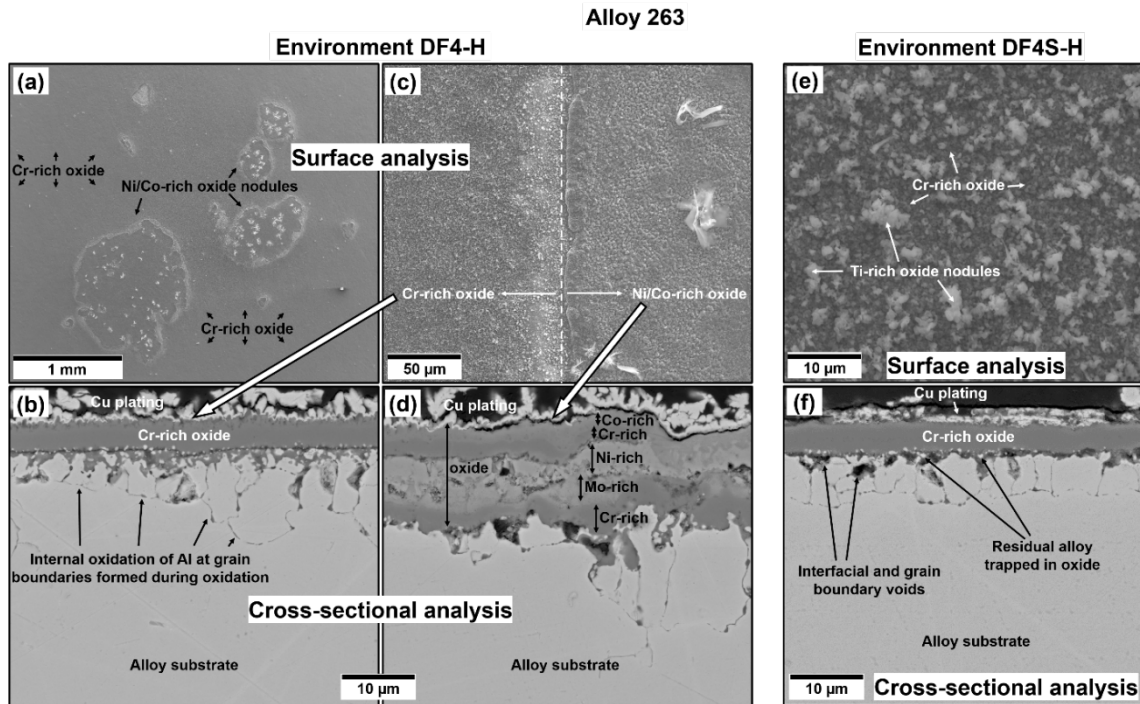


Figure 15. SEM analysis of alloy 263. (a-d) SE surface images and BSE cross-sectional images of coupon exposed to environment DF4-H. (e-f) SE surface image and BSE cross-sectional image of coupon exposed to environment DF4S-H. Both coupons imaged after 2,500 h. of exposure.

SEM surface images and EDS analysis of the coupon exposed to environment DF4-H revealed that while most of the surface was covered with a Cr-rich oxide, nodules of Ni- and Co-rich oxides were also observed sporadically across the surface. A cross-sectional image showing the Cr-oxide layer and the Ni/Co-rich oxide nodule are shown in Figure 15b and Figure 15d, respectively. While a single-layered Cr-rich oxide is observed for most of the surface (Figure 15b), the nodules are seen to consist of a multi-layer oxide structure and EDS confirmed the oxide layer contained Ni, Co, Mo, and Cr in the regions indicated in Figure 15d. Both an external and internal layer of Cr-rich oxide are observed in the multi-layer oxide structure, suggesting the scale was initially protective, followed by a stage of non-protective growth of Ni/Co/Mo oxides, before reestablishing growth of a protective Cr-rich oxide.

No such Ni/Co-rich oxide nodules were observed for the coupon exposed to environments DF4S-H, however small Ti-rich oxide nodules were observed across most of the surface (Figure 15e). Only a uniform Cr-rich oxide layer was observed for the entire cross-section of this coupon (Figure 15f) and the thickness of the oxide layer is not significantly different from the coupon exposed to environment DF4-H (Figure 15b).

Two additional features are seen in Figure 15b and Figure 15f which were present for most of the Ni alloys exposed to these environments. Firstly, internal oxidation of Al is observed which appears to be located preferentially along grain boundaries in the region immediately below the oxide layer. The observed intergranular oxidation suggests a grain size in this region that is significantly smaller than what would be expected for the unexposed alloy (average grain size  $\approx 95 \mu\text{m}$ ). This suggests that recrystallization of the alloy surface has occurred during the exposure. While it is possible that this process is related to the relief of residual stresses incurred by surface finishing (i.e., a purely temperature-driven effect), it has been proposed that this recrystallization is in fact related to the oxidation process. [8] Secondly, spots of bright contrast are observed near the bottom of the oxide layer, as labeled in Figure 15f. These are regions of residual alloy substrate which have been depleted of oxide-forming elements such as Cr and Al. It has been proposed that these regions are associated with the formation of interfacial voids which are then filled by oxidation, as described above.[8]

For all of the Ni alloys analyzed there was little or no evidence of sulfidation after exposure to environment DF4S-H. However, the presence of sulfides internally in the alloy cannot be unequivocally ruled out by this analysis because significant peak overlap of S and Mo in the X-ray spectra makes identifying S compounds in the alloy difficult using EDS. Additional analysis is planned to determine whether any sulfidation has occurred.

## SUMMARY

Several Fe and Ni commercial alloys, with potential use at high temperatures for both indirect and direct fired sCO<sub>2</sub> Brayton power cycle systems, were exposed at atmospheric pressure to temperatures and gases expected in a direct fired Allam cycle. This included exposures with and without SO<sub>2</sub> gas additions in the flowing gas stream. Gravimetric measurements on the coupons were made periodically to, or nearly to, 2,500 h. All the austenitic steels experienced minimal corrosion at 550 °C when no SO<sub>2</sub> was present. With 0.1 vol % SO<sub>2</sub> present it appears that more Cr was needed to maintain a long term stable oxide since both the lower Cr alloys, 304H and 347H, showed signs of breakaway corrosion at longer exposures. Both the ferritic steels GR 22 and GR 91 corroded relatively quickly at 550 °C, both with and without the presence of 0.1 vol % SO<sub>2</sub>, with the higher Cr GR 91 showing less mass gain than the GR 22. The presence of SO<sub>2</sub> only resulted in a relatively slight increase in mass gain over the tests without SO<sub>2</sub>. EDS showed the coupons tested at 550 °C with SO<sub>2</sub> in the gas stream had S present on their surfaces, presumably in the form of FeS.

The Ni alloys, which were exposed at 750 °C, showed only minor corrosion mass changes with an increase in gas stream water content or SO<sub>2</sub> being introduced to the gas stream. It is interesting that while the coupons were in a SO<sub>2</sub> environment no S compounds were found on or in the scale of the Ni alloys. The Ni based solution strengthened alloys generally did better than age hardenable alloys. This was particularly evident when comparing solution strengthened alloy 230 with age hardenable 263. The 230 had ¼, or less, the mass gain of the 263 at 2,500 h of exposure. Three other solution strengthened Ni alloys, 600, 617, 625, also showed low mass gain. The age hardenable 263 which had the highest mass gain for an Ni alloy in either DF11 or DF4S-H exposure. With the DF4-H exposure this alloy showed significant internal oxidation and poor stability of its outer scale. The Ni alloy with the most Fe, alloy 800, was the worst Ni alloy in the DF4-H exposure and was also next worst for the DF11 and DF4S-H exposures.

## ACKNOWLEDGMENTS

This work was performed in support of the US Department of Energy's Fossil Energy Crosscutting Technology Research Program. The Research was executed through NETL Research and Innovation Center's Advanced Alloy Development Field Work Proposal. Research performed by AECOM Staff was conducted under the RES contract DE-FE-0004000.

## DISCLAIMER

This report was prepared as an account of work sponsored by an agency of the United States Government. Neither the United States Government nor any agency thereof, nor any of their employees, makes any warranty, express or implied, or assumes any legal liability or responsibility for the accuracy, completeness, or usefulness of any information, apparatus, product, or process disclosed, or represents that its use would not infringe privately owned rights. Reference herein to any specific commercial product, process, or service by trade name, trademark, manufacturer, or otherwise does not necessarily constitute or imply its endorsement, recommendation, or favoring by the United States Government or any agency thereof. The views and opinions of authors expressed herein do not necessarily state or reflect those of the United States Government or any agency thereof.

## REFERENCES

- [1] Y. Ahn, S.J. Bae, M. Kim, S.K. Cho, S. Baik, J.I. Lee, J.E. Cha, Review of Supercritical CO<sub>2</sub> Power Cycle Technology and Current Status of Research and Development, *Nuclear Engineering and Technology*, 47 (6) (2015) 647-661.
- [2] F. Crespi, G. Gavagnin, S. D., G.S. Martinez, Supercritical Carbon Dioxide Cycles for Power Generation: a review, *Applied Energy*, 195 (2017) 152-183.
- [3] N. Weiland, R. Dennis, R. Ames, S. Lawson, P. Strakey, sCO<sub>2</sub> Cycles for Fossil Energy, Brown Univ., Providence, RI (United States). Dept. of Chemistry, 2017.
- [4] R.J. Allam, M. Palmer, G.W. Brown, System and Method for High Efficiency Power Generation using a Carbon Dioxide Circulating Working Fluid, Google Patents, 2010.
- [5] Y. Gong, D.J. Young, P. Kontis, Y.L. Chiu, H. Larsson, A. Shin, J.M. Pearson, M.P. Moody, R.C. Reed, On the Breakaway Oxidation of Fe<sub>9</sub>Cr<sub>1</sub>Mo Steel in High Pressure CO<sub>2</sub>, *Acta Materialia*, 130 (2017) 361-374.
- [6] P. Strakey, O. Dogan, G. Holcomb, G. Richards, Technology Needs for Fossil Fuel Supercritical CO<sub>2</sub> Power Systems, Proceeding of the 4<sup>th</sup> International Symposium Supercritical CO<sub>2</sub> Power Cycles, Pittsburgh, PA, USA, 2014.
- [7] R.D. Tarey, R.S. Rastogi, K.L. Chopra, Characterization of Thin Films by Glancing Incidence X-Ray Diffraction, *The Ragaku Journal*, 4 (1) (1987) 5.
- [8] R.P. Oleksak, C.S. Carney, G.R. Holcomb, Ö.N. Doğan, Structural Evolution of a Ni Alloy Surface During High-Temperature Oxidation, *Oxid Met*, (2017).
- [9] R.P. Oleksak, J.P. Baltrus, J. Nakano, A. Nakano, G.R. Holcomb, Ö.N. Doğan, Mechanistic Insights into the Oxidation Behavior of Ni Alloys in High-temperature CO<sub>2</sub>, *Corrosion Science*, 125 (2017) 77-86.